

Supramolecular Donor–Acceptor Heterojunctions by Vectorial Stepwise Assembly of Porphyrins and Coordination-Bonded Fullerene Arrays for Photocurrent Generation

Aiko Kira,[†] Tomokazu Umeyama,[†] Yoshihiro Matano,[†] Kaname Yoshida,[‡] Seiji Isoda,^{*,‡}
Jong Kang Park,[§] Dongho Kim,[§] and Hiroshi Imahori^{*,†,||,⊥}

Department of Molecular Engineering, Graduate School of Engineering, Kyoto University, Nishikyo-ku, Kyoto 615-8510, Japan, Institute for Chemical Research, Kyoto University, Uji, Kyoto 611-0011, Japan, Department of Chemistry, Yonsei University, Seoul 120-749, Korea, Institute for Integrated Cell-Material Sciences (iCeMS), Kyoto University, Nishikyo-ku, Kyoto 615-8510, Japan, and Fukui Institute for Fundamental Chemistry, Kyoto University, Sakyo-ku, Kyoto 606-8103, Japan

Received December 10, 2008; E-mail: isoda@eels.kuicr.kyoto-u.ac.jp; imahori@scl.kyoto-u.ac.jp

Bicontinuous donor–acceptor (D–A) arrays at the molecular level have attracted increasing scientific and technological interest because of their potential applications in organic photovoltaics.¹ Such D–A arrays would yield efficient charge separation (CS) and transportation of separated charges to their respective electrodes, leading to enhanced photocurrent generation provided that the vertical arrangement of the D–A arrays on the electrodes is ideal. Although nanostructures with bicontinuous D–A arrays have been obtained by self-assembly of D–A molecules,² it is still difficult to achieve the desirable vertical arrangement of bicontinuous D–A arrays on an electrode.³ Here we report a novel approach for constructing a vertical alignment of bicontinuous D–A arrays on a flat SnO₂ electrode for use as a photoelectrochemical device (Figure 1). A Pd-mediated stepwise self-assembly of zinc porphyrin (ZnP) donors ensures the vertical growth of porphyrin chains on the SnO₂ electrode.⁴ Pyridylfullerene (Py-C₆₀) acceptors are infiltrated into the porphyrin brush using coordination of the pyridyl moiety to the zinc atom together with π – π interactions between the Py-C₆₀ moieties.⁵ Therefore, we can systematically investigate the relationship between the film structure and the photoelectrochemical properties as a function of the number of porphyrin layers.

A SnO₂ electrode was modified with ZnP arrays as follows. A thin, nonporous SnO₂ film with a roughness factor of 1.1 was prepared on an FTO electrode.⁶ The assembly of ZnP arrays on the SnO₂ electrode was performed by a procedure similar to that described by Qian et al.^{4b} (Scheme S1 in the Supporting Information). First, pyridylporphyrin acid (Py-ZnP-acid; Figure S1) was adsorbed on the surface of the SnO₂ electrode through the carboxylic group. Next came Pd(II) coordination to the pyridyl group of the adsorbed Py-ZnP-acid followed by coordination of bis(pyridyl)porphyrin (ZnP-Py₂) to the Pd atom. The number of porphyrin layers could be controlled by the number of cycles of ZnP-Py₂ deposition via coordination between the pyridyl groups and Pd(II). Consequently, ZnP arrays were formed on the SnO₂ electrode; this structure is denoted as SnO₂/(ZnP)_n, where $n = 1–8$ is the number of porphyrin layers. Figure S2a displays UV–vis absorption spectra measured after each assembly of a porphyrin layer on the electrode. The absorption due to the porphyrin increased with the number of deposition cycles, implying the successive growth of porphyrin chains. The amount of assembled porphyrins exhibited a linear

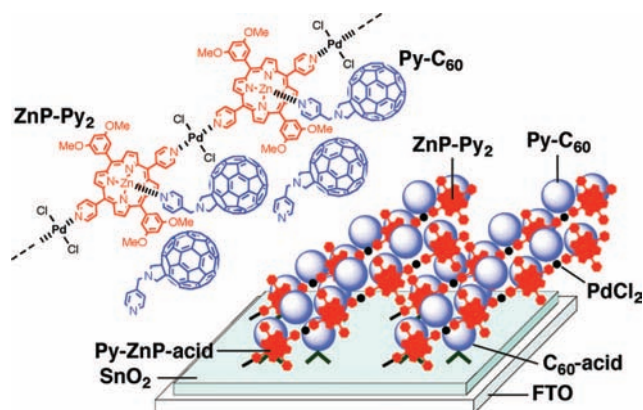


Figure 1. Schematic porphyrin–fullerene arrays on a SnO₂ electrode.

increase as the number of layers of porphyrins increased and leveled off at $n = 8$ (Figure S3).

Assembly of ZnP–C₆₀ composites was also performed on the SnO₂ electrode following Scheme S2 in the Supporting Information. First, Py-ZnP-acid and C₆₀-acid (Figure S1) were simultaneously adsorbed on the surface of the SnO₂ electrode, and then successive assembly of ZnP-Py₂ layers was achieved as described above (Figure S2b); this structure is denoted as SnO₂/C₆₀-acid+(ZnP)_n. In addition, the SnO₂/C₆₀-acid+(ZnP)_n electrodes were immersed into an *o*-dichlorobenzene (ODCB) solution of Py-C₆₀, which coordinated to the zinc porphyrins⁵ and became incorporated into the porphyrin arrays (yielding SnO₂/C₆₀-acid+(ZnP)_n+Py-C₆₀). Treatment of the SnO₂/C₆₀-acid+(ZnP)_n electrodes with the solution of Py-C₆₀ resulted in a significant rise in the absorption around 320–400 nm stemming from the absorption of Py-C₆₀ together with the red shift of the Soret band (Figure S4a).⁵ This demonstrates the complexation of Py-C₆₀ and ZnP and the infiltration of Py-C₆₀ from top to bottom in the ZnP brushes. The SnO₂/C₆₀-acid+(ZnP)_n electrodes were also treated with an ODCB solution of Ph-C₆₀ (Figure S1), which bears a phenyl rather than a pyridyl moiety. A slight rise in the absorption around 320–400 nm and no red shift were observed for the SnO₂/C₆₀-acid+(ZnP)_n+Ph-C₆₀ electrode, suggesting the weak interpenetration of Ph-C₆₀ into the ZnP arrays due solely to π – π interactions between Ph-C₆₀ units^{1c} (Figure S4b). The infiltrated amount of X-C₆₀ (X = Py, Ph) was determined by measuring the increase in absorbance of the electrodes at 375 nm resulting from the modification with X-C₆₀: [ZnP]/[Py-C₆₀] = 1:3 to 1:4 ($n = 2–6$) for the SnO₂/C₆₀-acid+(ZnP)_n+Py-C₆₀ electrodes

[†] Department of Molecular Engineering, Graduate School of Engineering, Kyoto University.

[‡] Institute for Chemical Research, Kyoto University.

[§] Yonsei University.

^{||} Institute for Integrated Cell-Material Sciences, Kyoto University.

[⊥] Fukui Institute for Fundamental Chemistry, Kyoto University.

and $[\text{ZnP}]/[\text{Ph-C}_{60}] = 1:1$ to $1:2$ ($n = 2-6$) for the $\text{SnO}_2/\text{C}_{60}\text{-acid}+(\text{ZnP})_n+\text{Ph-C}_{60}$ electrodes (Figure S5). The increased ratio for Py-C_{60} relative to Ph-C_{60} implies that the coordination in addition to the $\pi-\pi$ interactions contributes greatly to the infiltration. Steady-state fluorescence experiments revealed intense quenching of the porphyrin fluorescence for the $\text{SnO}_2/\text{C}_{60}\text{-acid}+(\text{ZnP})_n+\text{Py-C}_{60}$ electrodes compared with that of the reference without the C_{60} molecules (Figure S6). These results suggest that the porphyrin excited singlet state ($^1\text{ZnP}^*$) is quenched via electron transfer (ET) to the Py-C_{60} interpenetrated into the ZnP arrays.^{1c,2e,5} A weak emission around 700–800 nm may be attributed to the direct excitation of the C_{60} molecules incorporated into the ZnP arrays due to $\pi-\pi$ interactions between C_{60} molecules.⁷

The average thickness of the porphyrin arrays was evaluated using transmission electron microscopy (TEM) measurements on SnO_2 nanoparticles modified with the porphyrin arrays (Figure S7 in the Supporting Information). Close inspection of the TEM images showed that the thickness linearly increased as the number of porphyrin layers increased, indicating the linear elongation of the porphyrin chains. From a comparison of the film thicknesses and the lengths of the porphyrin arrays estimated from the sizes of porphyrins and Pd complexes (Table S1 and Figure S8), the orientation angle (θ) between the porphyrin arrays and the SnO_2 surface is estimated as $28 \pm 5^\circ$, which is consistent with the value for similar porphyrin arrays on quartz substrates.^{4b} A similar trend is noted for SnO_2 nanoparticles further modified with $\text{C}_{60}\text{-acid}$ and Py-C_{60} (Table S1). Atomic force microscopy (AFM) measurements were performed for the SnO_2 films modified with ZnP and C_{60} (Figure S9). The images of the $\text{SnO}_2/(\text{ZnP})_n$ and $\text{SnO}_2/\text{C}_{60}\text{-acid}+(\text{ZnP})_n+\text{Ph-C}_{60}$ substrates exhibited domain structures that would result from aggregation between the porphyrin chains, whereas those of the $\text{SnO}_2/\text{C}_{60}\text{-acid}+(\text{ZnP})_n+\text{Py-C}_{60}$ ($n = 2-5$) substrates disclosed a smooth surface morphology. In D–A blend films, such as conjugated polymer–fullerene derivative films in bulk heterojunction solar cells, an intimate mixing of the components leads to a smooth surface morphology of the film, which can be confirmed by using AFM.¹ Accordingly, the incorporation of Py-C_{60} molecules into the ZnP arrays suppresses the porphyrin aggregation, yielding the D–A bicontinuous arrays on the SnO_2 electrode.⁸

Figure S10 in the Supporting Information depicts the photocurrent action spectra for the modified electrodes, which closely resemble the corresponding absorption spectra of the electrodes (Figure S2). The incident photon-to-current efficiency (IPCE) and absorbed photon-to-current efficiency (APCE) values for the $\text{SnO}_2/(\text{ZnP})_n$ electrodes at 440 nm are plotted as functions of n in Figure 2a and Figure S11a, respectively. As n increased, both the IPCE and APCE values increased to reach maxima for $n = 3$ and then decreased gradually. As established previously,^{1c,2e,8} $^1\text{ZnP}^*$ injects electrons into the conduction band (CB) of SnO_2 , after which ET from I^- to the zinc porphyrin radical cation (ZnP^{*+}) occurs, generating a photocurrent (Scheme S3). The trend is reasonable, considering that the exciton diffusion length (~ 6 nm) of the porphyrin arrays, corresponding to the number of porphyrins and the total length ($n = 3$), is comparable to that of copper phthalocyanine (8 ± 3 nm) in bulk heterojunction solar cells.⁹ It is noteworthy that for the $\text{SnO}_2/\text{C}_{60}\text{-acid}+(\text{ZnP})_n+\text{Py-C}_{60}$ electrodes, the trends in the IPCE and APCE values as functions of n (Figures 2b and S11b) parallel that in the amount of Py-C_{60} infiltrated as a function of n .¹⁰ A similar trend is noted for the $\text{SnO}_2/\text{C}_{60}\text{-acid}+(\text{ZnP})_n+\text{Ph-C}_{60}$ electrodes.

The photodynamics of the photoinduced CS processes was studied by femtosecond time-resolved transient absorption measure-

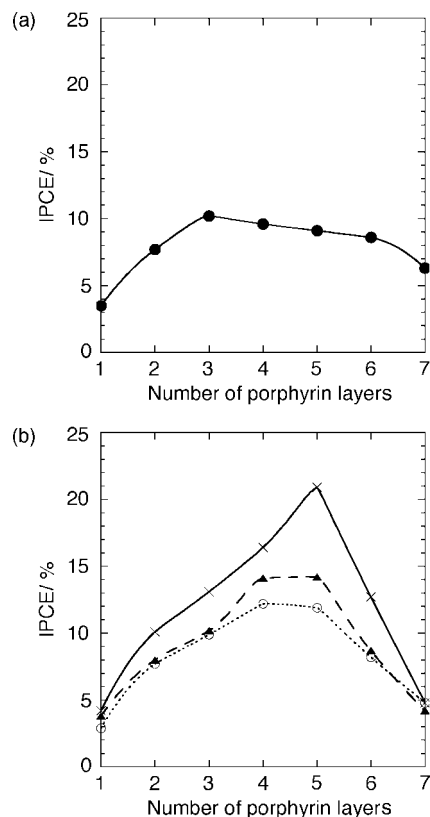


Figure 2. Plots of the IPCE values as functions of the number of porphyrin layers for (a) $\text{SnO}_2/(\text{ZnP})_n$ (solid line with filled circles) and (b) $\text{SnO}_2/\text{C}_{60}\text{-acid}+(\text{ZnP})_n+\text{Ph-C}_{60}$ (dotted line with open circles), $\text{SnO}_2/\text{C}_{60}\text{-acid}+(\text{ZnP})_n+\text{Py-C}_{60}$ (dashed line with triangles), and $\text{SnO}_2/\text{C}_{60}\text{-acid}+(\text{ZnP})_n+\text{Py-C}_{60}$ (solid line with crosses). Input power, $63 \mu\text{W cm}^{-2}$ ($\lambda_{\text{ex}} = 440$ nm); applied potential, 0.05 V vs SCE; 0.5 M LiI and 0.01 M I_2 in acetonitrile.

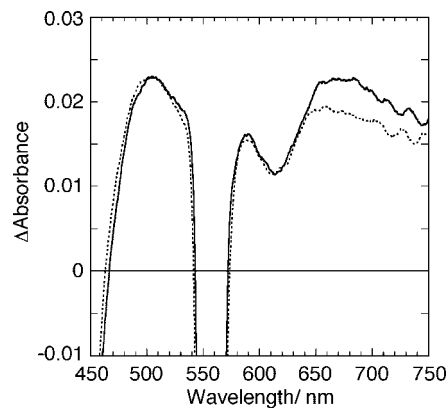
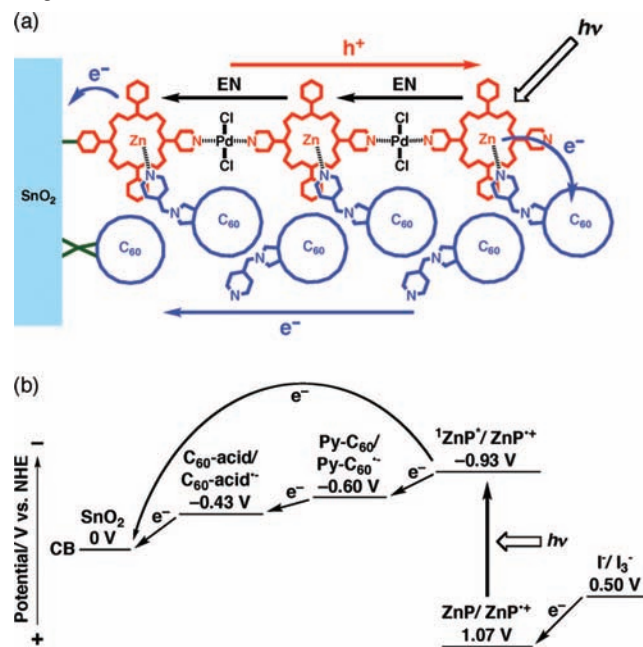


Figure 3. Transient absorption spectra of $\text{SnO}_2/\text{C}_{60}\text{-acid}+(\text{ZnP})_7+\text{Py-C}_{60}$ (solid line) and $\text{SnO}_2/(\text{ZnP})_7$ (dotted line) electrodes at time delay of 1 ps after laser excitation at 560 nm. The spectrum of the $\text{SnO}_2/(\text{ZnP})_7$ electrode was normalized to that of the $\text{SnO}_2/\text{C}_{60}\text{-acid}+(\text{ZnP})_7+\text{Py-C}_{60}$ electrode at 500 nm for comparison.

ments (Figure 3). The bleaching at 620 nm arises from $^1\text{ZnP}^*$,¹¹ whereas the broad absorption at ~ 660 nm originates from zinc porphyrin radical cation (ZnP^{*+}).¹¹ Although $^1\text{ZnP}^*$ and ZnP^{*+} appear simultaneously, the large Δ (absorbance) of $\text{SnO}_2/\text{C}_{60}\text{-acid}+(\text{ZnP})_7+\text{Py-C}_{60}$ relative to that of $\text{SnO}_2/(\text{ZnP})_7$ at ~ 660 nm exemplifies the additional contribution of the CS between ZnP and C_{60} to the enhancement in the photocurrent generation. This is consistent with the fact that the APCE value of the $\text{SnO}_2/\text{C}_{60}\text{-acid}+(\text{ZnP})_7+\text{Py-C}_{60}$ system (7.1% at 560 nm) is larger than that

Scheme 1. (a) Schematic Illustration of Photocurrent Generation in the $\text{SnO}_2/\text{C}_{60}\text{-acid}+(\text{ZnP})_n+\text{Py-C}_{60}$ System and (b) Its Energy Diagram^a



^a The levels of $\text{C}_{60}\text{-acid}$ and Py-C_{60} were determined electrochemically from the first reduction potentials of $\text{C}_{60}\text{-acid}$ and Py-C_{60} in chloroform.

of the $\text{SnO}_2/(\text{ZnP})_7$ system (5.0% at 560 nm). That is, exciton and carrier loss in the porphyrin arrays is suppressed as a result of exciton capture and charge dissociation by C_{60} , which can rationalize the fact that the maximum IPCE and APCE values were attained at a greater number of porphyrin layers for the $\text{SnO}_2/\text{C}_{60}\text{-acid}+(\text{ZnP})_n+\text{Py-C}_{60}$ system ($n = 5$) than for the $\text{SnO}_2/(\text{ZnP})_n$ system ($n = 3$). The decreasing trend of the IPCE and APCE values in the $\text{SnO}_2/\text{C}_{60}\text{-acid}+(\text{ZnP})_7+\text{Py-C}_{60}$ system for $n = 6-8$ correlates with the decreasing amount of C_{60} molecules incorporated between the porphyrin brushes, which arises from the porphyrin aggregation, as seen in the AFM measurements (see above).¹⁰ In such a case, the efficiency of CS between $^1\text{ZnP}^*$ and C_{60} would decrease with increasing n , leading to the decrease in the IPCE and APCE values. On the basis of the film structures and the photoelectrochemical properties of the $\text{SnO}_2/\text{C}_{60}\text{-acid}+(\text{ZnP})_n+\text{Py-C}_{60}$ systems together with the previously established photocurrent generation mechanism in similar porphyrin–fullerene composites on semiconducting electrodes,^{1c,2e,8} we can propose the photocurrent generation diagram shown in Scheme 1. First, CS between $^1\text{ZnP}^*$ and C_{60} takes place in addition to direct electron injection from $^1\text{ZnP}^*$ to the CB of the SnO_2 . In the former case, the generated $\text{C}_{60}^{\cdot-}$ injects electrons into the CB of the SnO_2 via electron hopping through the C_{60} molecules infiltrated from top to bottom in the porphyrin brushes. Thus, the bicontinuous D–A arrays for the $\text{SnO}_2/\text{C}_{60}\text{-acid}+(\text{ZnP})_n+\text{Py-C}_{60}$ ($n = 2-6$) electrodes are responsible for the enhancement of photocurrent generation.

In conclusion, we have successfully developed a novel strategy for constructing a vertical arrangement of D–A arrays on a

semiconducting electrode. The relationship between the film structure and photoelectrochemical properties has been elucidated as a function of the number of donor layers for the first time. The maximum IPCE value (21%) is comparable to the highest value (20%) reported for vertical arrangements of bicontinuous D–A arrays on electrodes.³ These results will provide fundamental clues for the molecular design of high-performance organic photovoltaics.

Acknowledgment. This work was supported by a Grant-in-Aid (19350068 to H.I.) and the WPI Initiative of MEXT, Japan. A.K. is grateful for a JSPS Fellowship for Young Scientists.

Supporting Information Available: Complete ref 2e, experimental details, Schemes S1–S3, Table S1, and Figures S1–S11. This material is available free of charge via the Internet at <http://pubs.acs.org>.

References

- (1) (a) Günes, S.; Neugebauer, H.; Sariciftci, N. S. *Chem. Rev.* **2007**, *107*, 1324. (b) Thompson, B. C.; Fréchet, J. M. J. *Angew. Chem., Int. Ed.* **2008**, *47*, 58. (c) Imahori, H. *J. Mater. Chem.* **2007**, *17*, 31. (d) Segura, J. L.; Martín, N.; Guldi, D. M. *Chem. Soc. Rev.* **2005**, *34*, 31.
- (2) (a) Schmidt-Mende, L.; Fechtenkötter, A.; Müllen, K.; Moons, E.; Friend, R. H.; MacKenzie, J. D. *Science* **2001**, *293*, 1119. (b) van der Boom, T.; Hayes, R. T.; Zhao, Y.; Bushard, P. J.; Weiss, E. A.; Wasielewski, M. R. *J. Am. Chem. Soc.* **2002**, *124*, 9582. (c) Würthner, F.; Chen, Z.; Hoeben, F. J. M.; Osswald, P.; You, C.-C.; Jonkheijm, P.; Herrikhuysen, J.; Schenning, A. P. H. J.; van der Schoot, P. P. A. M.; Meijer, E. W.; Beckers, E. H. A.; Meskers, S. C. J.; Janssen, R. A. J. *J. Am. Chem. Soc.* **2004**, *126*, 10611. (d) Sun, S.-S.; Zhang, C.; Ledbetter, A.; Choi, S.; Seo, K.; Bonner, C. E., Jr.; Drees, M.; Sariciftci, N. S. *Appl. Phys. Lett.* **2007**, *90*, 043117. (e) Imahori, H.; et al. *Chem.–Eur. J.* **2007**, *13*, 10182. (f) Li, W.-S.; Yamamoto, Y.; Fukushima, T.; Saeki, A.; Seki, S.; Tagawa, S.; Masunaga, H.; Sasaki, S.; Takata, M.; Aida, T. *J. Am. Chem. Soc.* **2008**, *130*, 8886. (g) Zhou, Z.; Chen, X.; Holderoft, S. *J. Am. Chem. Soc.* **2008**, *130*, 11711.
- (3) (a) Snaith, H. J.; Whiting, G. L.; Sun, B.; Greenham, N. C.; Huck, W. T. S.; Friend, R. H. *Nano Lett.* **2005**, *5*, 1653. (b) Sisson, A. L.; Sakai, N.; Banerji, N.; Fürstenberg, A.; Vauthey, E.; Matile, S. *Angew. Chem., Int. Ed.* **2008**, *47*, 3727.
- (4) (a) Drain, C. M.; Nifiatis, F.; Vasenko, A.; Batteas, J. D. *Angew. Chem., Int. Ed.* **1998**, *37*, 2344. (b) Qian, D.-J.; Nakamura, C.; Ishida, T.; Wenk, S.-O.; Wakayama, T.; Takeda, S.; Miyake, J. *Langmuir* **2002**, *18*, 10237.
- (5) (a) Troshin, P. A.; Koeppe, R.; Peregodov, A. S.; Peregodova, S. M.; Egginger, M.; Lyubovskaya, R. N.; Sariciftci, N. S. *Chem. Mater.* **2007**, *19*, 5363. (b) D'Souza, F.; Deviprasad, G. R.; Zandler, M. E.; Hoang, V. T.; Klykov, A.; Van Stipdonk, M.; Perera, A.; El-Khouly, M. E.; Fujitsuka, M.; Ito, O. *J. Phys. Chem. A* **2002**, *106*, 3243.
- (6) Acciarri, M.; Canevali, C.; Mari, C. M.; Mattoni, M.; Ruffo, R.; Scotti, R.; Morazzoni, F.; Barreca, D.; Armelao, L.; Tondello, E.; Bontempi, E.; Depero, L. E. *Chem. Mater.* **2003**, *15*, 2646.
- (7) The $\text{SnO}_2/\text{C}_{60}\text{-acid}+(\text{ZnP})_n+\text{Py-C}_{60}$ electrodes exhibited no characteristic emission around 800 nm due to charge transfer (CT) between ZnP and Py-C_{60} . This implies that no CT complexes are formed because the rather long separation distance between ZnP and Py-C_{60} caused by the coordination to Zn via the *N*-(4-pyridinylmethyl)pyrrolidine moiety does not allow the porphyrin moiety to make direct contact with the C_{60} molecules.^{5b}
- (8) (a) Imahori, H.; Liu, J.-C.; Hotta, H.; Kira, A.; Umeyama, T.; Matano, Y.; Li, G.; Ye, S.; Isosomppi, M.; Tkachenko, N. V.; Lemmetyinen, H. *J. Phys. Chem. B* **2005**, *109*, 18465. (b) Kira, A.; Tanaka, M.; Umeyama, T.; Matano, Y.; Yoshimoto, N.; Zhang, Y.; Ye, S.; Lehtivuori, H.; Tkachenko, N. V.; Lemmetyinen, H.; Imahori, H. *J. Phys. Chem. C* **2007**, *111*, 13618.
- (9) Peumans, P.; Yakimov, A.; Forrest, S. R. J. *Appl. Phys.* **2003**, *93*, 3693.
- (10) The slight difference in the maxima for the IPCE ($n = 5$) and the infiltrated amount of Py-C_{60} ($n = 6$) may result from the balance between porphyrin aggregation and C_{60} infiltration, as seen in Figure S9.
- (11) (a) Cho, Y.-J.; Ahn, T. K.; Song, H.; Kim, K. S.; Lee, C. Y.; Seo, W. S.; Lee, K.; Kim, S. K.; Kim, D.; Park, J. T. *J. Am. Chem. Soc.* **2005**, *127*, 2380. (b) Imahori, H.; Hagiwara, K.; Aoki, M.; Akiyama, T.; Taniuchi, S.; Okada, T.; Shirakawa, M.; Sakata, Y. *J. Am. Chem. Soc.* **1996**, *118*, 11771. (c) Luo, C.; Guldi, D. M.; Imahori, H.; Tamaki, K.; Sakata, Y. *J. Am. Chem. Soc.* **2000**, *122*, 6535. (d) Imahori, H.; Tamaki, K.; Guldi, D. M.; Luo, C.; Fujitsuka, M.; Ito, O.; Sakata, Y.; Fukuzumi, S. *J. Am. Chem. Soc.* **2001**, *123*, 2607.

JA8096465